Interference between One- and Two-Electron Channels in Resonant Inelastic X-Ray Scattering

Johan Söderström,[1,*] Marcus Agåker,[1,2] Ji-Cai Liu,[3,4,†] Takashi Tokushima,[2] Anirudha Ghosh,[2] Conny Såthe,[2] Jian Wang,[3,4] Andreas Pantelis Frey Koudouridis,[1] Moritz Grunwald-Delitz,[5] Thomas M. Baumann,[5] Michael Meyer,[5] Manuel Harder,[5] Zhong Yin,[6] Olle Björneholm,[1] Joseph Nordgren,[1] Stephan Fritzsche,[7,8,9] Victor Kimberg,[10,‡] Jan-Erik Rubensson,[1] and Faris Gel'mukhanov[10,11]

[1]*Department of Physics and Astronomy, Uppsala University, Box 516, 751 20 Uppsala, Sweden*
[2]*MAX IV Laboratory, Lund University, P.O. Box 118, SE-22100 Lund, Sweden*
[3]*School of Mathematics and Physics, North China Electric Power University, 102206 Beijing, China*
[4]*Hebei Key Laboratory of Physics and Energy Technology, North China Electric Power University, 071000 Baoding, China*
[5]*European XFEL, Holzkoppel 4, 22869 Schenefeld, Germany*
[6]*International Center for Synchrotron Radiation Innovation Smart, Tohoku University, Sendai 980-8572, Japan*
[7]*GSI Helmholtzzentrum für Schwerionenforschung, Planckstraße 1, 64291 Darmstadt, Germany*
[8]*Helmholtz-Institut Jena, Fröbelstieg 3, 07743 Jena, Germany*
[9]*Theoretisch-Physikalisches Institut, Friedrich-Schiller-Universität Jena, Max-Wien-Platz 1, 07743 Jena, Germany*
[10]*Theoretical Chemistry and Biology, KTH Royal Institute of Technology, SE-106 91 Stockholm, Sweden*
[11]*Helmholtz-Zentrum Berlin für Materialien und Energie, Institute for Methods and Instrumentation for Synchrotron Radiation Research, Albert-Einstein-Straße 15, D-12489 Berlin, Germany*

(Received 15 September 2025; accepted 27 October 2025; published 1 December 2025)

Interference between scattering channels is observed in resonant inelastic x-ray scattering (RIXS) at the Ne K threshold. Final states with $|2p^{-1}np\rangle$ as the main configuration are populated via $|1s^{-1}n'p\rangle$ resonances, where large-amplitude one-electron ($n' = n$) channels interfere with small-amplitude two-electron ($n' \neq n$) channels. The interference is manifested in an asymmetric line profile where the two-electron resonance occurs in the tail region of the one-electron resonance. In RIXS, this slowly varying tail plays the role of the continuum for the Fano effect. The asymmetric profile is well modeled by means of a single asymmetry parameter, determined by the amplitudes of the scattering channels and the energy separation between the resonances.

DOI: 10.1103/c5mk-trlz

Asymmetric spectral line shapes arise due to interference between a discrete resonance and a continuum, as originally described by Fano in the early 1960s [1]. The Fano effect is ubiquitous in resonant photoionization spectra of atoms, molecules, and materials with local excitations. In resonant inelastic x-ray scattering (RIXS) [2–4], on the other hand, final states situated below the ionization threshold preclude continuum interference as a mechanism for line-shape asymmetry. In this Letter, we analyze the observation of a Fano-like mechanism due to interference between two discrete resonances, as one resonance occurs on the slowly varying tail of another. This tail plays the role of the continuum for the classical Fano effect.

We investigate RIXS spectra excited at the Ne K edge, where $|2p^6\rangle \rightarrow |1s^{-1}n'p\rangle$ excitations are followed by $|1s^{-1}n'p\rangle \rightarrow |2p^{-1}np\rangle$ decay. One-electron decay ($n = n'$) interferes with two-electron decay ($n \neq n'$) where the $2p \rightarrow 1s$ transition is accompanied by a Rydberg electron shake process (Fig. 1). Because of this shake process, more than one scattering channel contributes to the population of the same final state,

$$\omega + |2p^6\rangle \rightarrow \left\{ \begin{array}{l} |1s^{-1}3p\rangle \\ |1s^{-1}4p\rangle \end{array} \right\} \rightarrow |2p^{-1}3p\rangle + \omega', \quad (1)$$

and consequently, one-electron-two-electron channel interference (OTCI) is expected. Here ω and ω' are the energies of incident and scattered radiation, respectively. The upper row is the one-electron RIXS channel where the initially excited Rydberg electron stays a spectator during the decay step, while the lower row is a two-electron channel, which opens due to Rydberg shake processes. In our spectra,

*Contact author: Johan.Soderstrom@physics.uu.se
†Contact author: jicailiu@ncepu.edu.cn
‡Contact author: kimberg@kth.se

OTCI is manifested in a Fano-like asymmetry in the cross section for populating specific states. We develop a theory that excellently describes the behavior in terms of a single q_L asymmetry parameter, determined by transition matrix elements, which we calculate from first principles.

While the neon atom is chosen as a prototype system, the results are relevant for RIXS spectra, in general, whenever there are two or more discrete excitation-emission pathways to the same final state. Such situations are common, e.g., for multiplet-split or chemically shifted resonances in atoms, molecules, and condensed matter.

The Fano effect is intrinsic in all photoionization processes, where resonances due to inner-shell excitations are embedded in the continuum of direct photoionization [6–8]. Interference between discrete states has primarily been investigated for vibrational sublevels [2], while much less attention has been paid to interference between discrete electronic states [2,8–11]. At close-to-threshold excitation, an initially excited Rydberg electron is subject to pronounced shake processes during the electronic decay, resulting in a wide distribution of final states [12]. This opens different pathways with comparable amplitudes to the same final state, and interference between discrete states must be taken into account to describe the threshold behavior. Typically, however, prominent continuum-bound Fano interference masks the interference between the discrete resonances in the electronic decay channel [8]. In RIXS, on the other hand, direct ionization into the photoelectron continuum can be neglected. In principle, the final states of the process can be reached via nonresonant inelastic scattering, corresponding the nonresonant channel in photoemission and implying a Fano-like behavior. However, the contribution of this process to the x-ray spectra is very small [13]. In the radiative decay channel, also the change in potential upon charge-conserving photon emission is small. Thus, Rydberg shake processes in the second step of the RIXS process are much less prominent [14] than in resonant photoemission, and threshold behavior has earlier been well described under the assumption that they can be neglected [15,16].

The experiment was performed at the Veritas beamline at the MAX IV synchrotron radiation facility. The large RIXS spectrometer [17] measured at 90° scattering angle in the horizontal plane, using a cylindrical grating with 67 m radius, and 1350 grooves/mm in the second order of diffraction. The incident radiation was polarized in the vertical plane. The combined resolution for spectrometer and beamline was measured via elastic scattering to be around 120 meV.

We used a cell with a 200 nm thick and 1 mm wide Si_3N_4 membrane to separate the sample gas at 1.0 bar from the ultrahigh vacuum. The incident and the emitted radiation penetrated the same membrane, the glancing angle of incidence being 30°. For the optically thick sample, we took saturation [18,19] into account for the predictions using the conditions described above, the x-ray absorption spectrum from Ref. [20] and absolute cross sections from Ref. [21]. Details are described in Supplemental Material [5].

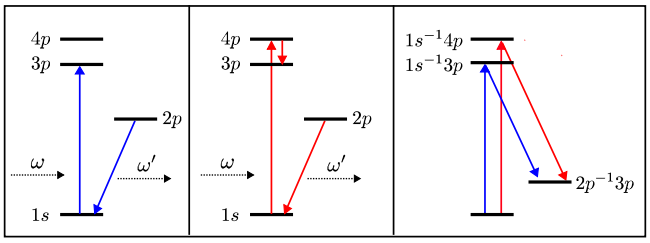

FIG. 1. Scheme of the transitions at the Ne K edge that we analyze in this Letter. As shown in Supplemental Material [5], the mechanism is general. Left: the one-electron transition where a $1s$ electron is excited to a $3p$ orbital, and the $1s$ vacancy is filled by an electron from the $2p$ orbital. Middle: the two-electron transition where a $1s$ electron is excited to a $4p$ orbital, and the filling of the $1s$ vacancy by an electron from the $2p$ orbital is accompanied by $4p \rightarrow 3p$ shake down. Right: the state representation of the same transitions: the $|2p^6\rangle \rightarrow |1s^{-1}3p\rangle \rightarrow |2p^{-1}3p\rangle$ channel (blue) populates the same final state as the $|2p^6\rangle \rightarrow |1s^{-1}4p\rangle \rightarrow |2p^{-1}3p\rangle$ channel (red), and the two channels interfere.

To model the inelastic scattering of x-rays, the multiconfiguration Dirac-Hartree-Fock (MCDHF) method has been applied to compute all second-order amplitudes in the resonant approximation. For atoms with inner-shell holes, in particular, the MCDHF method has been found versatile for systematically combining the excitation and emission process via the formation of different resonances [22], including the treatment of nonorthogonal sets of orbitals. To this end, we have expanded the Jena atomic calculator [23], to generate all many-electron amplitudes of the RIXS process including their relative phase. Emphasis has been placed to obtain a reasonable fine-structure splitting, even if the amplitudes themselves are slowly varying with details in the wave function expansion. We also performed a jj–LS recoupling to isolate the correct LS terms in the overall multiplet of singly excited neon atoms. While we shall not discuss details of the electronic structure calculations, the efficient implementation of the RIXS amplitudes is a key feature to quantitatively analyze these experiments.

At the Ne K edge, we consider $|2p^6\rangle \rightarrow |1s^{-1}n'p\rangle \rightarrow |2p^{-1}np(L)\rangle$ transitions (Fig. 1), where $|2p^6\rangle$ represents the $1s^22s^22p^{61}S_0$ ground state, and L refers to the orbital angular momentum of the final state. We can restrict the discussion to the singlet space since intercombination transitions into the triplet space are very weak for all light elements. Thus, only $|2p^6(^1S_0)\rangle \rightarrow {}^1P_1 \rightarrow {}^1S_0, {}^1P_1, {}^1D_2$ transitions are dipole allowed and, for simplicity, we refer to the final-state terms as S, P, D in the following.

Features corresponding to these transitions for low n and n' are marked in the two-dimensional (2D) RIXS map (Fig. 2). The vertical Raman ridges at constant energy loss

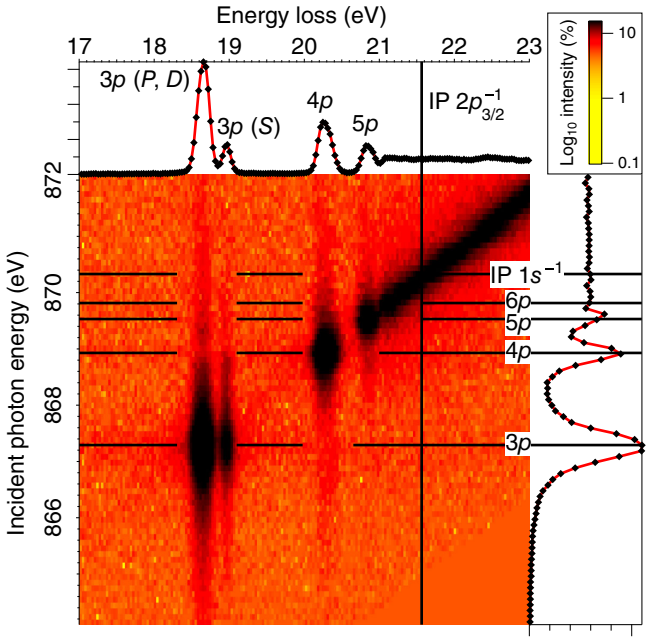

FIG. 2. 2D RIXS map (in logarithmic intensity scale) covering the Ne K edge, with projections on the energy-loss scale (top, linear intensity scale) and the resonance energy scale (right, linear intensity scale). Vertical Raman ridges correspond to the $|2p^{-1}np(L)\rangle$ final states, where for $n = 3$, states of $L = P$, D character are found at the energy loss $\omega - \omega' = 18.66$ eV, well separated from the $L = S$ state at 18.97 eV, and the unresolved multiplets of the $n = 4$ and $n = 5$ configurations are found at 20.28 and 20.85 eV energy loss, respectively. The resonance energies associated with $|1s^{-1}n'p\rangle$ states are marked with black horizontal lines for $n' = 3$, 4, 5, 6 at 867.29, 868.928, 869.530, and 869.815 eV, respectively [20] (21.565 [24] and 870.33 eV [20]). The ionization limits are also shown in the figure.

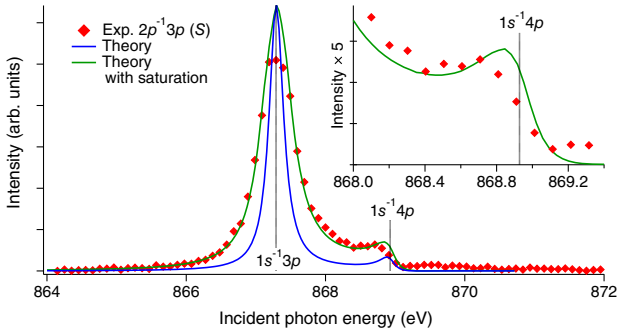

FIG. 3. The integrated intensity in the 18.88–19.08 eV energy interval (see Fig. 2) as a function of ω, reflecting the population of the $|2p^{-1}3p(S)\rangle$ final state (red dots). The predicted $\sigma_S(\omega)$ according to Eq. (2), using matrix elements calculated from first principles (blue), and the prediction including the saturation effect (green). The $|1s^{-1}3p\rangle$ and $|1s^{-1}4p\rangle$ resonance energies are marked with vertical dashed lines. Inset: enlarged part of the same data, highlighting the interference effects. The green and red curve are normalized to have the same area in the 864–871 eV range.

correspond to $|2p^{-1}np(L)\rangle$ final states, as the difference between the energy of the incoming radiation ω and the energy of the scattered radiation ω' is close to the final-state excitation energy, $\omega^{(L)}_{2pnp} \approx \omega - \omega'$. A projection onto the energy-loss axis is shown above the 2D map in Fig. 2. The $|2p^{-1}3p\rangle$ configuration shows two well-separated features: an intense ridge at 18.66 eV and a low-intensity ridge at 18.97 eV energy loss. The latter can be assigned to a $|2p^{-1}3p(S)\rangle$ state with almost pure S character. States with P and D character dominate the high-intensity ridge. For the unresolved $n = 4$ and 5 multiplets with maxima at 20.28 and 20.85 eV, respectively, the S, P, D splitting is only reflected in the width of the ridges (FWHM ≈ 0.2 eV). For higher n, the ridges converge to the continuum at 21.565 eV, and the $|2p^{-1}_{3/2}\epsilon\rangle$ final-state energies increase linearly with excitation energy, resulting in a diagonal band in the RIXS map.

We see sharp resonances especially in the lower n ridges, corresponding to $|1s^{-1}n'p\rangle$ resonances for $n' = 3$, 4, 5, and at higher n' the Rydberg resonances converge to the ionization limit at 870.33 eV [20]. The overall behavior is in line with earlier predictions [25], as well as experimental results [26]. We note in passing that RIXS data of this kind are wanted as a reference for free-electron-laser experiments, where this atom is typically used for benchmarking nonlinear x-ray processes like stimulated resonant Raman scattering [27–29].

For an isolated resonance ($n = n'$), e.g., $|2p^6\rangle \rightarrow |1s^{-1}3p\rangle \rightarrow |2p^{-1}3p\rangle$, one would expect a smooth, symmetric resonance curve, the projection on the excitation-energy scale of the ridge corresponding to the cross section for populating $|2p^{-1}3p\rangle$ final states.

In Fig. 2, however, we observe significant deviations from this behavior. There is obvious crosstalk between the ridges, e.g., we note a sharp variation of the $|2p^{-1}3p(L)\rangle$ intensity in the range where the excitation energy matches the $|1s^{-1}4p\rangle$ resonance. This behavior is further highlighted in Fig. 3, where the population of the $|2p^{-1}3p(S)\rangle$ final state is shown as a function of excitation energy. We see that the behavior is well described by the theoretical predictions.

The essence of the theory is that two interfering scattering channels [Eq. (1)] lead to the same $|2p^{-1}3p(L)\rangle$ final state. The amplitude for the two-electron transition $F_L^{(4p,3p)}$ is much smaller than the amplitude for the one-electron transition $F_L^{(3p,3p)}$. However, when ω is tuned near the $1s \rightarrow 4p$ resonance, the off-resonant one-electron channel becomes comparable to the resonant two-electron channel, resulting in pronounced OTCI.

We use the LS coupling scheme, which is fully justified for scattering to the S final state and lets us treat the other multiplets in an approximative fashion. For the sake of simplicity, we consider scattering to the $|2p^{-1}3p(S)\rangle$ states

in the main text and treat the general case in Supplemental Material [5], where we also explicitly derive the expressions for the scattering cross section written here,

$$\sigma_S(\omega,\omega') = \varrho_S \sigma_S(\omega)\delta(\omega-\omega'-\omega^{(S)}_{2p3p},\Gamma_f),$$
$$\sigma_S(\omega) = \frac{1}{3}\left|\frac{F_S^{(4p,3p)}}{\Omega+\imath\Gamma}+\frac{F_S^{(3p,3p)}}{\Omega+\Delta+\imath\Gamma}\right|^2 \quad (2)$$

in terms of the one- and two-electron amplitudes $F_S^{(3p,3p)}$ and $F_S^{(4p,3p)}$, which are equal to the product of the reduced transition dipole moments of the absorption and emission transitions (see Table I in Supplemental Material [5] for theoretical values),

$$F_S^{(3p,3p)} = \langle 0||d||1s^{-1}3p(P)\rangle\langle 1s^{-1}3p(P)||d||2p^{-1}3p(S)\rangle,$$
$$F_S^{(4p,3p)} = \langle 0||d||1s^{-1}4p(P)\rangle\langle 1s^{-1}4p(P)||d||2p^{-1}3p(S)\rangle.$$

The normalized Lorentzian $\delta(\omega-\omega'-\omega^{(S)}_{2p3p},\Gamma_f)$ with the width of the final state Γ_f describes the Raman dispersion, Γ is the lifetime broadening of the intermediate core excited state, $\Omega=\omega-\omega_{1s4p}$ is the detuning of the photon energy from the $1s\rightarrow 4p$ resonance, and $\Delta=\omega_{1s4p}-\omega_{1s3p}$ is the difference between the resonant energies $\omega_{1sn'p}$.

The polarization prefactor ϱ_L in Eq. (2) explicitly takes the angular dependence into account and motivates the chosen experimental geometry. In general, it can be written in terms of the polarization vectors of incident $\mathbf{e}$ and scattered $\mathbf{e}'$ photons and the Clebsch-Gordan coefficients: $\varrho_L = 3\sum_M|\sum_{\mu\mu_1} e^{\mu}e'^{\mu_1}C^{00}_{1M'1\mu}C^{1M'}_{LM1\mu_1}|^2$. For scattering to S, P, and D final states, we get

$$\varrho_S=(\mathbf{e}\cdot\mathbf{e}')^2,\quad \varrho_P=(\mathbf{e}\times\mathbf{e}')^2,$$
$$\varrho_D=\frac{1}{5}[9-7(\mathbf{e}\cdot\mathbf{e}')^2]. \quad (3)$$

Our spectrometer is not sensitive to the polarization of the scattered radiation, and we average the cross section over rotations of $\mathbf{e}'$ around the direction of the momentum $\mathbf{k}'$ of the scattered photon using $\overline{(\mathbf{e}\cdot\mathbf{e}')^2}=\frac{1}{2}[1-(\mathbf{e}\cdot\hat{\mathbf{k}}')^2]$ and $\overline{(\mathbf{e}\times\mathbf{e}')^2}=1-\overline{(\mathbf{e}\cdot\mathbf{e}')^2}$, where $\hat{\mathbf{k}}'=\mathbf{k}'/k$. In the experiment, we use vertical polarization of the incident radiation, and 90° scattering angle, implying that $\angle(\mathbf{e},\mathbf{k}')=90°$, and we obtain $\varrho_S=1/2$, $\varrho_P=1/4$, and $\varrho_D=11/10$. In contrast, horizontal polarization would have implied $\varrho_S=0$, and scattering to S final states would not have been observed.

We use two alternative representations of the integral RIXS cross section that highlight different aspects of the process. First, we separate the cross section [Eq. (2)] in direct and interference terms,

$$\sigma_S(\omega)=\sigma_S^{\mathrm{dir}}(\omega)+\sigma_S^{\mathrm{int}}(\omega), \quad (4)$$

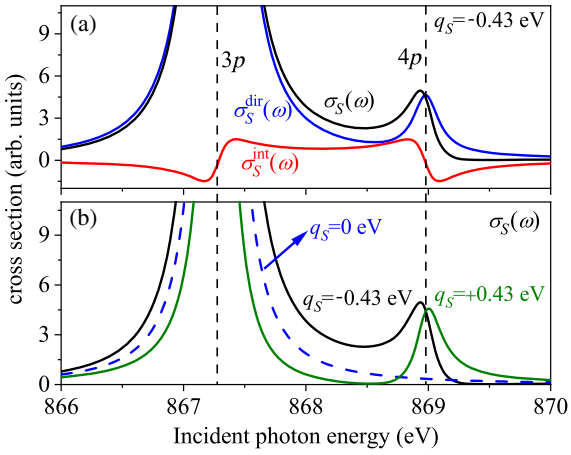

FIG. 4. (a) Direct $\sigma_S^{\mathrm{dir}}(\omega)$ term (blue), interference $\sigma_S^{\mathrm{int}}(\omega)$ term (red), and the resulting total cross section $\sigma_S(\omega)$ (black) [see Eq. (4)], using theoretical matrix elements, which give $q_S=-0.43$ eV. (b) $\sigma_S(\omega)$ [Eq. (5)] for $q_S=-0.43$ eV (black) compared to the hypothetical case where $q_S=+0.43$ (green) and $q_S=0$ (dashed), which restores a symmetric Lorentzian centered at the $|1s^{-1}3p\rangle$ resonance. The resonance energies are marked with vertical dashed lines.

where $\sigma_S^{\mathrm{dir}}(\omega)$ is the sum of the square modulus of two- and one-electron contributions in expression (2) for $\sigma_S(\omega)$, while $\sigma_S^{\mathrm{int}}(\omega)$ is the interference term (see Supplemental Material [5]).

This conventional expression demonstrates that interference contributes to the intensity between the resonances [Fig. 4(a)], in line with earlier observations of interference in the electronic decay channel [6,9]. In RIXS, the steep variation at the resonances can be unambiguously assigned to the interference between the discrete states as the nonresonant scattering channel can be neglected. The variation has the largest impact at the weak two-electron channel resonance and gives it an asymmetric Fano-like shape.

For the comparison between the predictions and the experimental results in Fig. 3, we have accounted for saturation effects arising because our medium is optically thick (see Supplemental Material [5] for details). Saturation relatively suppresses the intense features and enhances the weak. It makes the main $|1s^{-1}3p\rangle$ peak much broader (FWHM ≈ 0.7 eV) than what is expected from the intrinsic width (FWHM ≈ 0.25 eV), and it relatively increases the intensity of the asymmetric feature at the $|1s^{-1}4p\rangle$ resonance.

The second expression for $\sigma_S(\omega)$ underlines the resemblance between OTCI and Fano interference; the role of the Fano continuum is played by the smooth tail of the strong one-electron channel,

$$\sigma_S(\omega)=A\frac{(\Omega+q_S)^2+\Gamma^2}{(\Omega^2+\Gamma^2)[(\Omega+\Delta)^2+\Gamma^2]}. \quad (5)$$

Here $A = (F_S^{(3p,3p)} + F_S^{(4p,3p)})^2/3$. The asymmetry parameter $q_S = F_S^{(4p,3p)}/(F_S^{(3p,3p)} + F_S^{(4p,3p)})\Delta$ explains the observed strong asymmetry due to the two-electron transition at the $|1s^{-1}4p\rangle$ resonance (Fig. 3).

In Fig. 4(b), we show how the shape of the resonance [Eq. (5)] varies with q_L. The asymmetry critically depends, not only on the magnitude of q_L, but also on its sign, which is determined by the sign of the scattering amplitudes. While the RIXS cross section can often be understood in terms of the absolute square of the electronic matrix elements, the type of phase sensitivity manifested here is inherent when interference is important. This is widely exploited for vibrational wave functions in lifetime-vibrational interference effects [2,3,30], which become especially prominent when the vibrational spacing in the intermediate state is small compared to the lifetime width. In contrast, OTCI relies on a large spacing between the interfering intermediate electronic states as $q_L \propto \Delta$. Sensitivity to the phase of the photon wave function in recent observations of Young-double-slit interference [31–33] gives indirect sensitivity to the phase of the electronic wave functions. However, a direct observation of the relative phases of two coherently excited discrete electronic states in a RIXS experiment has not been reported before.

We also observe OTCI in scattering to $|2p^{-1}3p\rangle$ states of P and D character at the $|1s^{-1}4p\rangle$ resonance and also in scattering to $|2p^{-1}4p\rangle$ and $|2p^{-1}5p\rangle$ final states at the $|1s^{-1}3p\rangle$ resonance. The analysis follows the same line as the analysis above, and we refer to Supplemental Material [5] for details about the general treatment.

We note that $q_L = F_L^{((n+1)p,np)}/\left(F_L^{(np,np)} + F_L^{((n+1)p,np)}\right)\Delta \to 0$ as n increases toward threshold where $\Delta \to 0$. OTCI will thus be unimportant in the immediate vicinity of threshold. Although several strongly overlapping $|1s^{-1}n'p\rangle$ Rydberg states are simultaneously excited in the first step, no interference effects in the RIXS process are expected. This is in sharp contrast to resonant Auger spectroscopy, where a multitude of interfering electronic decay channels contribute and develop into postcollision interaction in the continuum [12].

A threshold behavior in the present experiment that may seem intriguing at first sight is the substantial population of neutral final states several eV above the $1s$ ionization limit at 870.33 eV (Fig. 2). The $n = 3$ intensity is particularly strong, but also $n = 4$, 5, 6 final-state population stretches above the ionization limit. A faint diagonal line of intensity below the main resonances indicates that also $2p^{-1}\epsilon$ continuum states are populated below the ionization limit. This behavior is not due to nonresonant inelastic scattering or intricate threshold dynamics. It can be understood in terms of the same RIXS processes that have been discussed throughout the Letter and is merely a consequence of long Lorentzian tails due to the finite lifetime of the core hole states. Saturation relatively enhances the weaker spectral features.

In conclusion, we have measured and analyzed the threshold behavior of RIXS at the Ne K edge. We find interference between scattering channels where $|2p^{-1}np(L)\rangle$ final states are populated at $|1s^{-1}n'p\rangle$ resonances, also for $n' \neq n$. Especially, the two-electron channel where $n' = 4$ and $n = 3$ interferes strongly with the one-electron channel where $n = n' = 3$. This one-electron-two-electron channel interference leads to a Fano-like asymmetry close to the $|1s^{-1}4p\rangle$ resonance. We develop a general theory that excellently describes the behavior in terms of a parameter q_L, determined by the amplitudes for the excitation-emission channels and the energy difference between the resonances.

Acknowledgments—O. B. acknowledges support from the Swedish Research Council (VR Project No. 2023-04346). J.-E. R. acknowledges support from the Swedish Research Council (VR Project No. 2021-04017). J. N. acknowledges the Carl Trygger Foundation for financial support. J.-C. L. and J. W. acknowledge National Natural Science Foundation of China under Grants No. 12211530044 and No. 11974108. V. K. acknowledges STINT Mobility Grants for Internationalisation (Project No. MG2021-9085). M. H. acknowledges funding by the German Federal Ministry of Education and Research under Grant No. 13K22XXB DYLUXIT. The authors are grateful to Dr. Alfred Müller for gracefully providing the unsaturated Ne $1s^{-1}$ x-ray absorption spectrum shown in Fig. 2 in the Supplemental Material [5], this spectrum was originally published in Ref. [20]. We acknowledge the MAX IV Laboratory for beamtime on the Veritas beamline under proposal 20240293. Research conducted at MAX IV, a Swedish national user facility, is supported by Vetenskapsrådet (Swedish Research Council, VR) under Contract No. 2018-07152, Vinnova (Swedish Governmental Agency for Innovation Systems) under Contract No. 2018-04969 and Formas under Contract No. 2019-02496.

Data availability—The data that support the findings of this article are openly available [34].

[1] U. Fano, Phys. Rev. **124**, 1866 (1961).
[2] F. Gel'mukhanov, M. Odelius, S. P. Polyutov, A. Föhlisch, and V. Kimberg, Rev. Mod. Phys. **93**, 035001 (2021).
[3] J. Stöhr, 1st ed., *The Nature of X-Rays and Their Interactions with Matter* (Springer, New York, 2023).
[4] F. M. F. de Groot, M. W. Haverkort, H. Elnaggar, A. Juhin, K.-J. Zhou, and P. Glatzel, Nat. Rev. Methods Primers **4**, 45 (2024).
[5] See Supplemental Material at http://link.aps.org/supplemental/10.1103/c5mk-trlz for where the saturation effects are calculated and compared to the absorption coefficient, a general derivation of the OTCI theory are described together with calculated transition matrix

elements. Furthermore, OTCI from other final state population are also shown here.

[6] R. Camilloni, M. Žitnik, C. Comicioli, K. C. Prince, M. Zacchigna, C. Crotti, C. Ottaviani, C. Quaresima, P. Perfetti, and G. Stefani, Phys. Rev. Lett. **77**, 2646 (1996).

[7] R. R. T. Marinho, O. Björneholm, S. L. Sorensen, I. Hjelte, S. Sundin, M. Bässler, S. Svensson, and A. Naves de Brito, Phys. Rev. A **63**, 032514 (2001).

[8] A. De Fanis, N. Saito, H. Yoshida, Y. Senba, Y. Tamenori, H. Ohashi, H. Tanaka, and K. Ueda, Phys. Rev. Lett. **89**, 243001 (2002).

[9] J.-E. Rubensson, M. Neeb, A. Bringer, M. Biermann, and W. Eberhardt, Chem. Phys. Lett. **257**, 447 (1996).

[10] E. Kukk, G. Snell, J. D. Bozek, W.-T. Cheng, and N. Berrah, Phys. Rev. A **63**, 062702 (2001).

[11] F. Gel'mukhanov, J.-C. Liu, P. Krasnov, N. Ignatova, J.-E. Rubensson, and V. Kimberg, Phys. Rev. A **108**, 052820 (2023).

[12] H. Aksela, M. Kivilompolo, E. Nõmmiste, and S. Aksela, Phys. Rev. Lett. **79**, 4970 (1997).

[13] Y.-P. Sun, Q. Miao, A. Pietzsch, F. Hennies, T. Schmitt, V. N. Strocov, J. Andersson, B. Kennedy, J. Schlappa, A. Föhlisch, F. Gel'mukhanov, and J.-E. Rubensson, Phys. Rev. Lett. **110**, 223001 (2013).

[14] G. B. Armen, J. Phys. B **24**, 2467 (1991).

[15] J. Söderström, M. Alagia, R. Richter, S. Stranges, M. Agåker, M. Ström, S. Sorensen, and J.-E. Rubensson, J. Electron Spectrosc. Relat. Phenom. **141**, 161 (2004).

[16] J.-E. Rubensson, J. Söderström, C. Binggeli, J. Gråsjö, J. Andersson, C. Såthe, F. Hennies, V. Bisogni, Y. Huang, P. Olalde, T. Schmitt, V. N. Strocov, A. Föhlisch, B. Kennedy, and A. Pietzsch, Phys. Rev. Lett. **114**, 133001 (2015).

[17] M. Agåker, C.-J. Englund, V. Ekholm, L. Kjellsson, P. Sjöblom, L. Pickworth, J. Söderström, N. Johansson, A. Ghosh, T. Tokushima, M. Caputo, J. Forsberg, G. Felcsuti, P. Fredriksson, S. Malki, N. Wassdahl, C. Såthe, and J.-E. Rubensson, J. Synchrotron Radiat. **32**, 1328 (2025).

[18] J. Stöhr, *NEXAFS Spectroscopy* (Springer, Berlin, Heidelberg, 1992).

[19] S. Eisebitt, T. Böske, J.-E. Rubensson, and W. Eberhardt, Phys. Rev. B **47**, 14103 (1993).

[20] A. Müller, D. Bernhardt, A. Borovik, T. Buhr, J. Hellhund, K. Holste, A. L. D. Kilcoyne, S. Klumpp, M. Martins, S. Ricz, J. Seltmann, J. Viefhaus, and S. Schippers, Astrophys. J. **836**, 166 (2017).

[21] I. H. Suzuki and N. Saito, J. Electron Spectrosc. Relat. Phenom. **129**, 71 (2003).

[22] S. Fritzsche, Atoms **10**, 127 (2022).

[23] S. Fritzsche, Comput. Phys. Commun. **240**, 1 (2019).

[24] Victor Kaufman and Lennart Minnhagen, J. Opt. Soc. Am. **62**, 92 (1972).

[25] A. N. Khoperskiĭ, A. M. Nadolinskiĭ, R. V. Koneev, and V. A. Yavna, Opt. Spectrosc. **100**, 510 (2006).

[26] M. Oura, Plasma Sci. Technol. **12**, 353 (2010).

[27] C. Weninger and N. Rohringer, Phys. Rev. A **88**, 053421 (2013).

[28] U. Eichmann *et al.*, Science **369**, 1630 (2020).

[29] K. Li *et al.*, Nature (London) **643**, 662 (2025).

[30] F. Gel'mukhanov and H. Ågren, Phys. Rep. **312**, 87 (1999).

[31] A. Revelli, M. M. Sala, G. Monaco, P. Becker, L. Bohatý, M. Hermanns, T. C. Koethe, T. Fröhlich, P. Warzanowski, T. Lorenz, S. V. Streltsov, P. H. M. van Loosdrecht, D. I. Khomskii, J. van den Brink, and M. Grüninger, Sci. Adv. **5**, eaav4020 (2019).

[32] M. Magnaterra, M. Moretti Sala, G. Monaco, P. Becker, M. Hermanns, P. Warzanowski, T. Lorenz, D. I. Khomskii, P. H. M. van Loosdrecht, J. van den Brink, and M. Grüninger, Phys. Rev. Res. **5**, 013167 (2023).

[33] J. Söderström, A. Ghosh, L. Kjellsson, V. Ekholm, T. Tokushima, C. Såthe, N. Velasquez, M. Simon, O. Björneholm, L. Duda, A. N. de Brito, M. Odelius, J.-C. Liu, J. Wang, V. Kimberg, M. Agåker, J.-E. Rubensson, and F. Gel'mukhanov, Sci. Adv. **10**, eadk3114 (2024).

[34] J. Söderström, Zenodo (2025), 10.5281/zenodo.14714286.